ELSEVIER

Chemical Engineering Journal 81 (2001) 91–100

Chemical Engineering Journal

www.elsevier.com/locate/cej

Kinetics identification of salicylic acid precipitation through experiments in a batch stirred vessel and a T-mixer

A.F. Blandin [a,*], D. Mangin [a], V. Nallet [a], J.P. Klein [a], J.M. Bossoutrot [b]

[a] *LAGEP, UMR CNRS 5007, Université Claude Bernard, Lyon 1, ESCPE-Lyon, 43 Boulevard du 11 Novembre 1918, F69622 Villeurbanne Cedex, France*

[b] *Centre de Recherches Rhône-Alpes, Elf Atochem, Rue Henri Moissan, BP 20, F69491 Pierre Bénite Cedex, France*

Accepted 24 July 2000

Abstract

This work aims to identify the mechanisms and kinetics of salicylic acid precipitation. A large supersaturation domain is covered (initial supersaturation ratios between 2.7 and 65.0) and two experimental set-ups are used. At low supersaturations, precipitations are performed in a stirred vessel, whereas a T-mixer must be used at high supersaturations in order to avoid hydrodynamic effects. In each case, the precipitation mechanisms actually involved are different and their kinetics are identified by solving the population balance with the method of classes. Thus, at low supersaturations in the stirred vessel, the primary nucleation is of heterogeneous type and the secondary nucleation is dominant, whereas homogeneous primary nucleation dominates in the T-mixer at high supersaturations. The crystal growth is diffusion controlled in the stirred vessel and turns into an integration limited mechanism in the T-mixer.

Keywords: Precipitation; Kinetics; Modeling; T-mixer; Salicylic acid

1. Introduction

The knowledge of the kinetics of the different crystallization mechanisms is essential to reliably scale-up industrial precipitation equipment. However, a poor agreement of the kinetics found in literature for a same compound is frequently observed. Indeed, the studied mechanisms greatly depend on the operating conditions [1]. For instance, Mersmann [2] pointed out that the growth rate derived from growth measurements on an *individual crystal* using a growth cell differs from the crystal growth rate derived from a *crystal collective* present in an industrial crystallizer. Likewise, Tavare [3] could not compare the kinetics of salicylic acid precipitation he obtained to those published by Franck et al. [4] or Al-Kayat [5] because the experimental protocols were too different.

The dependence on the operating conditions is intensified in case of precipitation reactions because of the high supersaturation levels that can be reached locally. Indeed, it is not only the kinetics but also the dominating mechanisms of a given crystallization process which strongly depend on the supersaturation level [6]. Moreover, at high supersaturation levels, the solid formation and more precisely the primary nucleation occurs very rapidly and its time scale can become of the same order of magnitude as the kinetics of mixing. In this case, macro- and micro-mixing greatly influence the final crystal size distribution (CSD) and precipitation is seriously affected by hydrodynamics. Thus, in order to obtain the correct kinetic parameters, particular attention must be paid to make the precipitation free from any mixing effects [7].

The methods to evaluate kinetics from experimental data are numerous and can be divided into two groups [8]. The first kind of methods is based on the experimental isolation of the two simultaneous processes: nucleation and crystal growth. For instance, Eble [9] carried out aluminum hydroxides precipitations in a Y-mixer combined with a stirred vessel in order to separate nucleation from crystal growth and agglomeration. However, the experimental isolation of the two mechanisms is not always possible. Thus, in a similar experimental set-up, but at lower supersaturation levels, Mignon [10] found that the crystal size distribution of strontium sulfate obtained at the T-mixer outlet is due to simultaneous nucleation and crystal growth. To separate the different mechanisms contributions, it is then necessary to use a mathematical model treatment. This corresponds to the second group of methods. A widely used approach con-

* Corresponding author. Tel.: +33-472-431-856; fax: +33-472-431-699.
E-mail address: blandin@lagep.univ-lyon1.fr (A.F. Blandin).

1385-8947/01/$ – see front matter
PII: S1385-8947(00)00227-8

Nomenclature

A_I, B_I	kinetic parameters of primary nucleation (nb m^{-3} s^{-1}), (–)
A_{II}, B_{II}	kinetic parameters of secondary nucleation (nb m^{-2} s^{-1}), (–)
$\mathcal{A}$	kinetic parameters set derived from batch experiments
$\mathcal{B}$	kinetic parameters set derived from T-mixer experiments
C_c	crystal molar density (mol m^{-3})
C^*_{RH}	salicylic acid solubility (mol m^{-3})
C_{RH}	molar concentration of salicylic acid (mol m^{-3})
C^0_{RH}	initial molar concentration of salicylic acid (mol m^{-3})
CV_{nb}	coefficient of variation of the CSD in number (–)
$f = L1/L2$	lengthening factor (–)
G	growth rate (m s^{-1})
j	integration growth rate exponent (–)
J_I, J_{II}	primary and secondary nucleation rates (nb m^3 s^{-1})
k	Boltzmann constant (J K^{-1})
k_c	integration growth rate factor (mol^{1-j} m^{3j-2} s^{-1})
k_d	mass transfer coefficient (m s^{-1})
$L1$, $L2$	length and width of parallepipedic crystals (m)
L	characteristic size of crystals (m)
L^*	critical size of the nuclei (m)
L_{nb}	crystals mean size in number (m)
M_s	molecular weight of solid (kg mol^{-1})
N_t	total number of crystals per volume unit of suspension (nb m^{-3})
Q_e, Q_s	inlet, outlet volumetric flow rates (m^3 s^{-1})
Q_r	reactants volumetric flow rate (mm^3 s^{-1})
S	total surface of crystals per volume unit of suspension (m^2 m^{-3})
t	time (s)
T	temperature (K)
v	molecular volume (m^3)

Greek letters

β	supersaturation ratio (–)
β^0	initial supersaturation ratio (–)
γ_{sl}	interfacial tension between solid and liquid phase (J m^{-2})
δ	Dirac delta function
η_r	effectiveness factor (–)
ρ_s	solid density (kg m^{-3})
Φ_s, Φ_v	surface and volumetric shape factors (–)
Ψ	population density function (nb m^{-1} m^{-3})

sists then in solving the population balance equation which involves the different mechanisms. Once more, there are several numerical ways for solving that population balance equation and they can be classified in three main sub-cases [11]. The method of moments [12] is based on the evaluation of the crystal size distribution moments. But it is impossible to access the real distribution from the moments and the result given by the model is then much poorer than the experimental data. The accuracy in the determination of the kinetic parameters may so be affected because not the whole experimental information is used. This may explain why the kinetic parameters of salicylic acid precipitation proposed by Franck et al. [4] cannot correctly represent our experimental data obtained under similar operating conditions. The methods of the second sub-case consist in decomposing the population density function on a set of polynomial and orthogonal functions [13] and the results are expressed in terms of continuous CSDs. The last methods are based on a size discretization of the population balance equation. This leads to a set of ordinary differential equations with a number of equations equal to the number of granulometric classes. Then, either the partial derivatives of the population density function are calculated [14] or the differential equations are integrated along with the size to obtain differential equations with absolute numbers of crystals in each class (method of classes, introduced by Marchal et al. [15]).

Starting from all these elements, we develop in this study an original method to identify precipitation kinetics. First, determining kinetics of precipitation needs to cover a large supersaturation domain. The study follows then two steps: (i) at low initial supersaturation ratios, batch precipitations are carried out in a perfectly mixed vessel by adding quickly the second reactant to the first one; (ii) for high initial supersaturation ratios, precipitations are performed in a T-mixer in order to minimize mixing effects. Thus, for initial supersaturation ratios exceeding 3.4 in the stirred vessel, the batch precipitation goes through a step during which the suspension is pseudoplastic gel-like; the suspension is then badly mixed and no reproducibility in crystal size distribution can be obtained. The use of a T-mixer allows one to better control the reactants mixing and consequently, the supersaturation coming out and the nucleation rate.

In both configurations, hydrodynamic and kinetic models are developed. The precipitation mechanisms taken into account are homogeneous and heterogeneous primary nucleation, surface secondary nucleation, chemical and diffusion controlled growth. The population balance equation is then solved using the method of classes.

For each of the supersaturation levels studied, the kinetic parameters of the dominating mechanisms are identified by matching experimental and simulated results. Eventually, the dominant mechanisms in the batch experiments at low supersaturations are compared to those which prevail at high supersaturations in the T-mixer.

2. Experimental study

2.1. Materials

Salicylic acid is an intermediate product in the manufacturing of acetylsalicylic acid or aspirin. Owing to its weak solubility, salicylic acid is industrially produced by neutralization of sodium salicylate by sulfuric acid. The chemical reaction leads to a soluble molecule which then crystallizes.

$$H_2SO_4 + H_2O \rightarrow HSO_4^- + H_3O^+ \quad (1)$$

$$HSO_4^- + H_2O \Leftrightarrow SO_4^{2-} + H_3O^+ \quad (2)$$

$$2R^- + 2H_3O^+ \Leftrightarrow 2RH_{soluble} + H_2O \quad (3)$$

$$2RH_{soluble} \rightarrow 2RH \downarrow \text{(precipitate)} \quad (4)$$

where R^- is the salicylate ion and RH the salicylic acid.

The chemical equilibria (2) and (3) are assumed to be reached instantaneously compared with the crystallization (4) kinetic. Salicylic acid precipitates as prismatic needle or rod shaped crystals.

2.2. Experiments

2.2.1. At low initial supersaturation ratio: batch precipitations in a stirred vessel

The precipitations are performed in a 2.5×10^{-3} m^3 jacketed glass precipitator equipped with four baffles and stirred by a profiled propeller of type TT from Mixel Company (France) [16]. The sulfuric acid solution is quickly added into the precipitator which initially contains a solution of sodium salicylate. All the experiments are carried out without seeding at 25°C and with a stirring speed of 300 rpm which corresponds to a specific power input of 0.3 W kg^{-1}; the excess of initial sulfuric acid was taken equal to 1.2 times the stoichiometric ratio. Three experiments were performed with initial concentrations of sodium salicylate of 40, 45 and 50 mol m^{-3} which give initial supersaturation ratios ($\beta^0 = C^0_{RH}/C^*_{RH}$) of 2.7, 3.0 and 3.4, respectively.

With these experimental conditions, calculated macro- and micro-mixing time are lower than 3 s [17], whereas the experimental induction times are over 70 s. Thus it can be assumed that the mixing is instantaneous and that the precipitation occurs in a perfectly mixed reactor.

2.2.2. At high initial supersaturation ratio: precipitations in a T-mixer

A scheme of the experimental set-up [16] is shown in Fig. 1. The T-mixer, made of glass, is an opposed flow T with two identical arms of 165 mm in length and 1 mm in (inner) diameter. Its outlet tube (i.e. mixing pipe) has a length of 363 mm and an internal diameter of 1.8 mm. In order to improve macro- and micro-mixings a small sphere acting as a mixing chamber was designed just below the confluence of the two arms. The volume of this sphere is about 160 mm^3.

The two reactants solutions feed respectively each of the two arms of the T. The initial concentration of sodium salicylate ranging from 750 to 1750 mol m^{-3} (i.e. β^0 from 27.4 to 65.0). The reactants flow rates (Q_r) are equal and fixed so that the precipitation is not affected by mixing effects. Indeed, evaluations of the macro-mixing time using colored flows showed that, if the reactants flow rates are high enough ($Q_r > 2.0$ mm^3 s^{-1}), the macro-mixing occurred in the small sphere. Besides, calculated micro-mixing times in the mixing chamber [17] are of the same order of magnitude as the residence time in that chamber or slightly lower than it. The reactants micro-mixing is already important in the sphere. This is confirmed by acid–base neutralization experiments in the presence of colored indicator which showed that the micro-mixing was achieved in that sphere. The residence time in the following mixing tube is about 10 times higher than that in the mixing chamber.

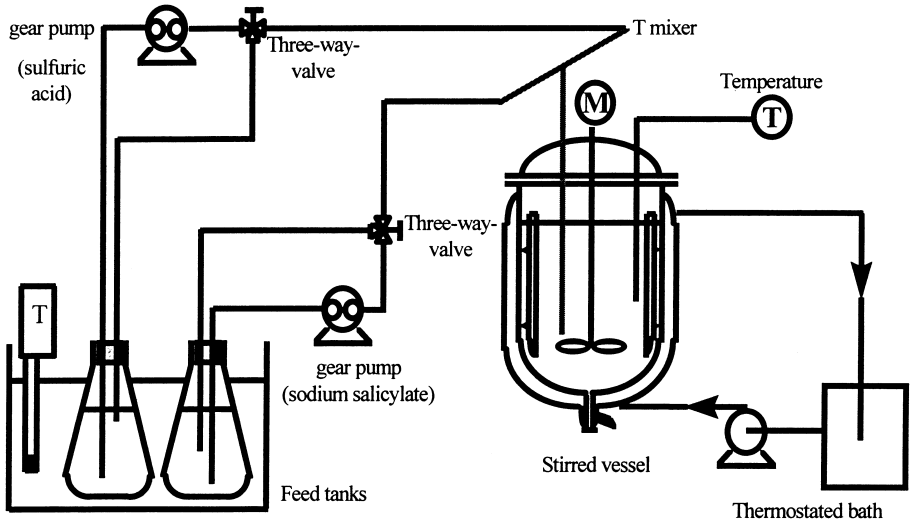

Fig. 1. Experimental set-up for high initial supersaturation level precipitations.

The precipitation takes place in the mixing chamber and in the mixing tube. The suspension stemmed from the T-mixer flows out into a stirred vessel similar to that used for the batch experiments. The vessel is previously filled with $1.7 \times 10^{-3}\,m^3$ of water saturated with salicylic acid in order to reduce the supersaturation and the further nucleation spontaneously. The exit of the T is located just over the turbine. The crystallization finishes in that vessel.

2.3. Measurements

2.3.1. Supersaturation

In *batch precipitations*, owing to the high conductivity of H_3O^+, the conductivity of the solution can be assumed to be proportional to the concentration of H_3O^+ ions. Therefore, the concentration of H_3O^+ and afterwards, the concentrations of all other species present in the precipitator can be calculated due to the conservation and the equilibrium relationships. Particularly, the supersaturation is known as a function of time [18]. For the precipitations performed in a T-mixer, such a measurement is not available.

2.3.2. Crystal size distribution

At the end of the batch precipitations performed in the stirred vessel, a representative sample is withdrawn from the suspension and filtered on black membranes.

For T-mixer precipitations, two kinds of samples are withdrawn: (i) at the T-exit and (ii) from the stirred vessel at the end of the crystallization process. The T-exit samples are obtained by directly filtering the suspension at the outlet of the T-mixer. A large amount of iced water is then added to the suspension before the filtration, in order to dilute the suspension and to stop the crystallization processes without dissolving the crystals.

In both cases, the monocrystals are measured and counted by using an optical microscope coupled with an image analysis software. They are assimilated to square base parallelepipeds and 2 sizes ($L1$, $L2$, $L1 > L2$) are then measured to obtain the equivalent diameter L of the sphere of the same volume. This size L is taken as the characteristic size of the crystals. No significant agglomeration was observed on these samples.

Table 1
Batch precipitations in the stirred vessel — final CSDs characteristics and total number of crystals obtained in batch precipitation

β^0 (–)	L_{nb} (μm)	CV_{nb} (%)	$f = L1/L2$ (–)	$N_t \times 10^{-9}$ (nb m^{-3})
2.7	102.1	45.2	4.50	2.6
3.0	89.7	43.4	4.51	4.7
3.4	75.2	47.8	6.02	8.6

2.4. Experimental results

Tables 1 and 2 summarize the main characteristics of the CSDs obtained from both configurations. L_{nb} is the average size in number of the crystals, CV_{nb} is the variation coefficient of the CSD and f is the average lengthening factor. The CSDs were all determined by counting 500 crystals. We have also reported the total number of crystals per volume unit (N_t) obtained at the end of the crystallization process. In both cases, N_t is calculated from the final CSD and the total mass of crystallized salicylic acid itself evaluated through a mass balance.

From these tables, it can be seen that the total number of crystals strongly depends on the initial supersaturation level. This means that nucleation is very sensitive to supersaturation, which should lead to a good accuracy in the identification of the nucleation law parameters.

The evolution of the shape factor (f) is also interesting. Indeed it appears in Table 2 that f does not exceed 2.2 for the micro-crystals produced in the T-mixer. For larger crystals produced by batch precipitations, f is much higher (Table 1). This confirms that organic crystals deformation occurs as they grow.

Finally, it is worth observing that crystals at the T-exit are smaller than crystals which have stayed in the vessel (Fig. 2). This means that the crystallization is not finished at the T-exit.

3. Modeling and simulation

The model for salicylic acid precipitation is based on:

- the description of hydrodynamics,

Table 2
Precipitations in the T-mixer — total number of crystals and CSDs characteristics obtained at T-mixer exit and in the vessel acting as a finisher

β^0	$Q_r \times 10^6$ (m^3 s^{-1})	T-exit			Vessel			
		L_{nb} (μm)	CV_{nb} (%)	f (–)	L_{nb} (μm)	CV_{nb} (%)	f (–)	$N_t \times 10^{-14}$ (nb m^{-3})
27.4	2.36	3.8	37.9	2.20	5.6	38.2	2.11	0.84
	4.80	4.0	37.7	2.07	4.8	42.3	2.05	1.19
46.3	2.36	3.0	37.3	1.98	5.0	41.7	1.97	1.72
	4.80	3.0	38.8	1.99	5.1	36.6	1.94	1.84
65.0	2.36	2.7	47.2	1.83	4.0	57.9	2.04	3.24
	4.80	1.8	32.1	1.80	4.1	53.4	1.93	3.42

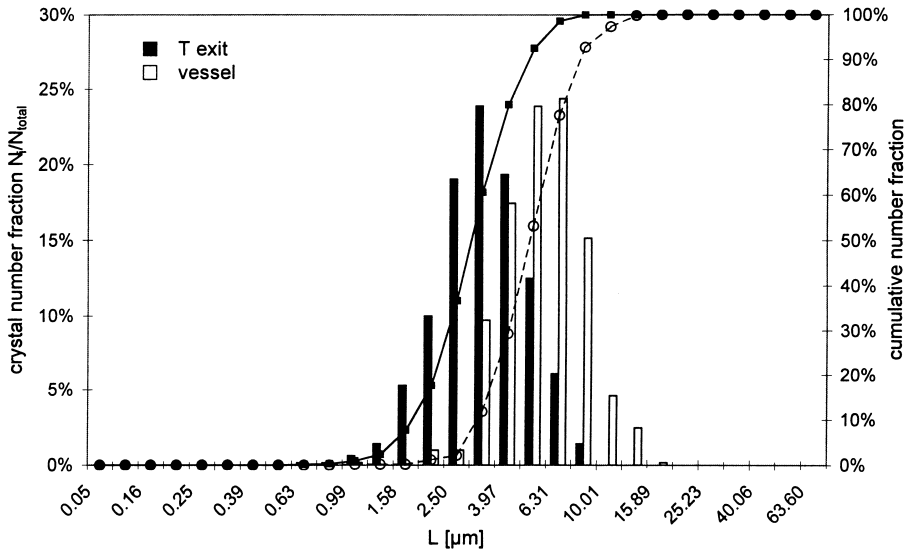

Fig. 2. Precipitation in T-mixer — comparison between the CSD at the T-exit and the CSD in the vessel at the end of the crystallization. β^0: 46.3 and Q_r: 4.80 mm^3 s^{-1}.

- mass balances and equilibrium relationships,
- kinetics of the crystallization processes,
- the population balance giving the CSD which is the key part of the model.

3.1. Model

3.1.1. Hydrodynamic model

The stirred vessel used in the two experimental set-ups is considered as perfectly mixed. As concerns the T-mixer, the mixing chamber located just below the confluence of the two arms of the T, is assimilated to a perfectly mixed continuous reactor. The mixing tube which follows this chamber is modeled by a perfect plug flow reactor.

3.1.2. Mass balances and equilibrium relationships

The system is made up of seven species, including Na^+ and the precipitate RH↓. Four relationships between the species and the solid concentrations are derived from electroneutrality and mass balances on R, Na and SO_4 radicals. Two other relationships are given by the equilibrium relationships describing the acids dissociation. This leads to a system of six equations and seven unknown variables. The seventh condition necessary to solve the problem is given by the population balance.

3.1.3. Crystallization kinetic laws

Primary nucleation. The following well-known expression [19] has been used where A_I and B_I are semi-empirical parameters:

$$J_{NI} = A_I \exp\left[\frac{-B_I}{(\ln\beta)^2}\right] \quad (5)$$

Secondary nucleation. The secondary nucleation is described by a surface mechanism assuming a two-dimensional nucleation mechanism on the surface S of the crystals already present [6,18]:

$$J_{NII} = A_{II} S \exp\left[\frac{-B_{II}}{\ln\beta}\right] \quad (6)$$

where A_{II} and B_{II} are semi-empirical parameters.

Crystal growth. Crystalline growth is described by the film model with a mass transfer process across the diffusion layer surrounding the crystal, in competition with the surface integration mechanism of the solute molecule into the crystal.

$$G = \frac{dL}{dt} = \frac{\Phi_s M_s k_c}{3\rho_s \Phi_v} \eta_r (C_{RH} - C^*_{RH})^j \quad (7)$$

where η_r is the effectiveness factor introduced by Garside [20], solution of

$$\left[\frac{k_c}{k_d}(C_{RH} - C^*_{RH})^{j-1}\right]\eta_r + \eta_r^{1/j} - 1 = 0 \quad (8)$$

k_d is evaluated in the perfectly mixed batch reactor with the correlation of Herndl and Mersmann [21] and in the T-mixer, with the correlation of Armenante and Kirwan [22] established for micro-particles, i.e. particles whose size is comparable to or smaller than the Kolmogorov minimum eddy size. k_c and j are semi-empirical parameters.

Agglomeration. In this study, no significant agglomeration was observed. Moreover, since the optical microscope enabled us to directly measure the monocrystals, the agglomeration mechanism were not taken into account in the model.

3.1.4. Population balances

The population of crystals is described by the number density function Ψ ($\Psi(L, t)\,dL$ is the number of crystals of size between L and $L + dL$ per unit volume at time t). The instantaneous balance of crystals of size between L and $L + dL$ during the time dt can be written as

$$\frac{1}{V(t)}\frac{\partial[\Psi(L,t)V(t)]}{\partial t} + \frac{\partial[\Psi(L,t)G(L,t)]}{\partial L} + \frac{Q_s\Psi_s(L,t) - Q_e\Psi_e(L,t)}{V(t)} = [J_{NI}(t) + J_{NII}(t)]\delta(L - L^*(t)) \quad (9)$$

where V is the reactor volume, Q_e and Q_s the inlet and outlet volumetric flow rates, δ the Dirac delta function, $J_{NI}\delta(L-L^*)$ and $J_{NII}\delta(L-L^*)$ the primary and secondary nucleation rate density functions, L^* the size of the nuclei linked to the supersaturation according to the Gibbs–Thomson equation:

$$L^*(t) = \frac{2v\gamma_{sl}}{kT\ln(\beta(t))} \quad (10)$$

The balance equation (9) is then adapted to each reactor used. For instance, the T-mixer is modeled in steady state only. However, in the simulation program, the steady state of the perfectly mixed continuous reactor, at the T-mixer entrance, is given by the asymptote of the transient state and it is then necessary to solve an instantaneous balance. Then the plug flow reactor is fed with the suspension stemmed from the mixed reactor only when the latter is in steady state; the population balance, in this plug flow reactor, is written for a differential volume element and the variable t corresponds to the internal age of the molecules at the entrance of the volume element of interest.

In all cases, the partial differential equation (9) is discretized by using the method of classes [5,9] to generate a system of ordinary differential equations. This system coupled with the mass balance and the kinetic equations is solved by calling an adaptive step fifth order Runge–Kutta method which optimizes the precision and the integration speed [10]. In the general case, the complete model involves six kinetic parameters.

3.2. Identification

In both cases, it is difficult to analyze the identifiability of the parameters on a strict mathematical point of view. Our approach is rather pragmatic. First, although the isolation of the different mechanisms is done by solving the population balance equation, it is clear that the experimental data available must be rich enough to allow the evaluation of the different kinetics. As far as the batch experiments are concerned, for instance, the total number of crystals produced by primary and secondary nucleations is given by the final CSD. The isolation of the two mechanisms is possible thanks to the supersaturation versus time curve since the primary nucleation is strongly linked to the induction time. The slope of that same curve and the final crystal size are governed by the growth rate. As concerns the T-mixer experiments, it is obvious that without any experimental results at the T-exit, we cannot separate the nucleation and growth contributions in the T-mixer. Mignon et al. [10] separates those two contributions by measuring the total time of the precipitation process.

Secondly, the sensitivity of the simulated results towards each parameter is studied in order to confirm the relevance of the experimental data available. Once the identifiability of the kinetic parameters is checked, an optimization procedure using a modified Levenberg and Marquardt algorithm, coupled to the intelligent use of some physical insight into the system, is used to iterate on the kinetic parameters values until the simulated results best fit the experimental ones.

3.2.1. Simulations at low supersaturations

The experiments carried out in the perfectly mixed batch reactor with the initial supersaturation ratio β^0 between 2.7 and 3.4 have allowed to identify the following optimal set of kinetic parameters [5]:

$$\text{set } \mathcal{A}: \quad A_I = 0.55 \times 10^9 (\text{nb m}^{-3}\,\text{s}^{-1}), \quad B_I = 4.4\,(-)$$
$$A_{II} = 0.99 \times 10^8 (\text{nb m}^{-2}\,\text{s}^{-1}), \quad B_{II} = 4.8\,(-)$$
$$k_c = 0.23 \times 10^{-3} (\text{mol}^{-1}\,\text{m}^4\,\text{s}^{-1}), \quad j = 2\,(-)$$

Fig. 3 shows the agreement obtained between model and experimental data for an initial ratio of 3.0. Similar agreement is obtained for the other experiments. Simulations with these parameters show that, in the studied supersaturation domain, secondary nucleation has a greater contribution than primary nucleation since about 70% of the total number of nuclei are then produced by secondary nucleation. The low value of parameter $B1$ indicates that the primary nucleation mechanism is probably of heterogeneous type. Besides, growth is essentially diffusion controlled, so the accuracy of the kinetic growth parameters (k_c, j) describing integration step is low.

3.2.2. Simulations at high supersaturations

3.2.2.1. Simulation with the parameters set $\mathcal{A}$. The kinetic parameters determined at low supersaturations (set $\mathcal{A}$) have been injected in the T-mixer simulation program. However, they cannot represent the experiments. In particular, the simulated number of produced crystals is much too small. For example, the simulated number is only equal to 10^8 (crystals) m^{-3} while the expected number was of 1.72×10^{14} (crystals) m^{-3} for the experiment carried out with an initial supersaturation ratio of 46.3 and a flow rate of $2.36 \times 10^{-6}\,\text{m}^3\,\text{s}^{-1}$ for each reactant. This failure of the parameters $\mathcal{A}$ is probably due to the high difference in supersaturation levels that exists between the two kinds of experiments. Indeed, because of the high levels of supersaturation used, primary nucleation in the T-mixer is probably of homogeneous type whereas a heterogeneous mechanism must be dominant at low supersaturation levels in the batch

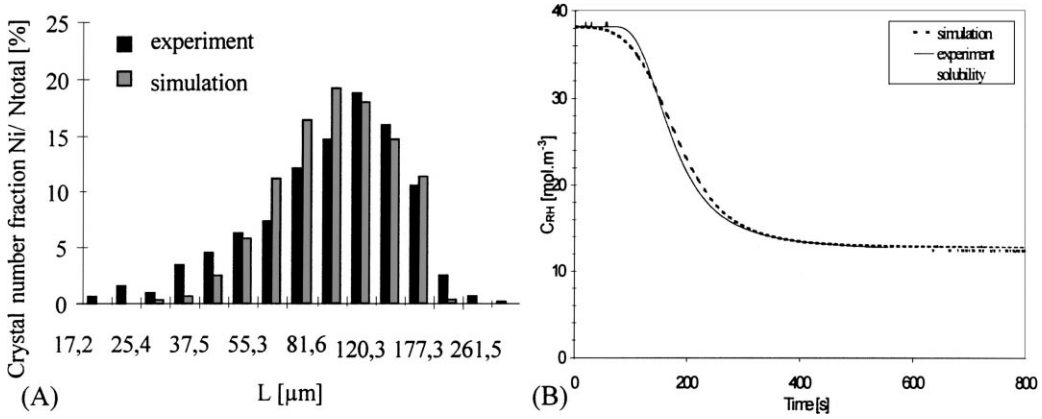

Fig. 3. Batch precipitation — comparison between model and experimental data (A) crystal size distribution, (B) concentration of dissolved salicylic acid vs. time.

precipitator. Thus, the kinetic parameters of the homogeneous primary nucleation have to be determined by using the T-mixer experiments.

3.2.2.2. Identification of new kinetic parameters. For T-mixer precipitations, the simulated CSD is very sensitive to the integration growth parameters. Preliminary simulations showed that the growth parameters of set $\mathcal{A}$ determined from the batch mixed reactor experiments with a low precision generate too high simulated growth rates. Thus, the kinetic growth parameters need also to be redetermined. On the contrary, the secondary nucleation parameters of set $\mathcal{A}$ are conserved. The heterogeneous primary nucleation is not introduced in the model since, as seen before, it is negligible compared with the homogeneous primary nucleation. In conclusion, (A_I, B_I) relating the new kinetic of homogeneous nucleation and (k_c, j) have to be identified from the T-mixer experiments. These parameters are determined by matching the simulated and experimental final CSDs obtained in the vessel. The simulated and experimental CSDs have to be in good accordance at the T-exit too.

Finally, the following parameters set leads to simulations representing satisfactorily the T-mixer experiments:

$$\text{set } \mathcal{B}: \quad A_I = 12 \times 10^{17} (\text{nb m}^{-3}\,\text{s}^{-1}), \quad B_I = 80\,(-)$$
$$k_c = 2.5 \times 10^{-4} (\text{m s}^{-1}), \qquad j = 1\,(-)$$

It is worth observing that the value proposed here for B_I is greater than that of set $\mathcal{A}$, which is in accordance with the hypothesis of a primary nucleation mechanism of homogeneous type in the T-mixer. Besides, B_I is close to the theoretical value that can be calculated from the expression of homogeneous primary nucleation proposed by Mersmann [6].

Examples of the agreement between experimental and predicted final CSD are given in Fig. 4. The difference observed between the two CSDs on the smallest classes can be explained since such particles cannot be seen nor measured. In fact, these submicronic particles were not taken into account to optimize the kinetic parameters. It was more delicate to match the CSDs at the T-exit since the fine particles were more numerous at that stage and only the biggest

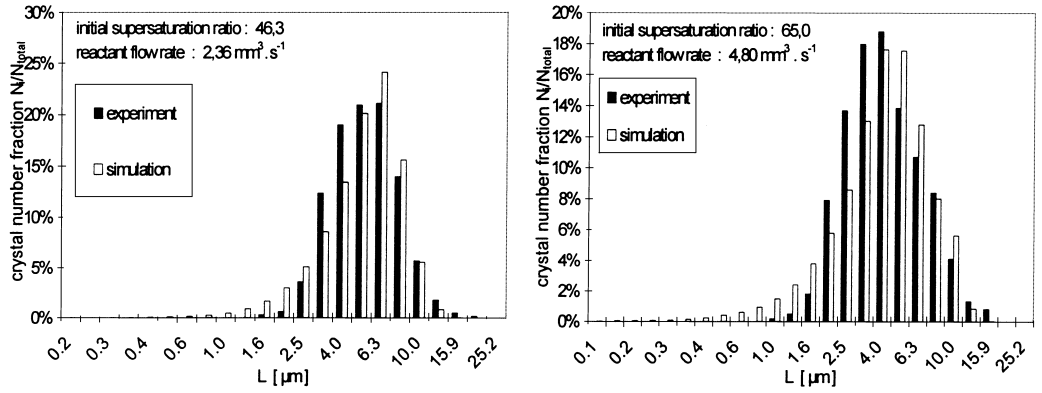

Fig. 4. T-mixer precipitations — comparison between experimental and simulated CSD after 45 min in the stirred vessel for two different initial supersaturation ratios.

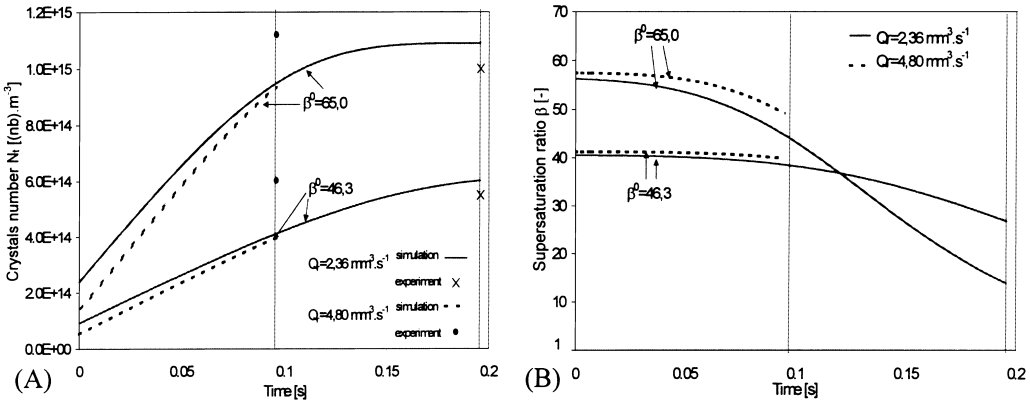

Fig. 5. Precipitations in T-mixer. (A) Experimental crystal number at the T-exit and simulated crystal number vs. time in the perfect plug flow reactor. (B) Simulated supersaturation vs. time in the perfect plug flow reactor.

particles were then considered for the identification. The parameters identification by matching the CSDs only at the T-exit would have been therefore insufficient.

The simulation results give some interesting insight into the phenomena occurring during the T-mixer precipitation. Thus, the evolution of the simulated supersaturation presented in Fig. 5(B) shows that precipitations are not finished at the T-exit, which is in good accordance with experiments (Fig. 2). However, it appears on Fig. 6 that supersaturation is quickly consumed in the stirred vessel since the highest value reached for $Q_r = 4.80\,mm^3\,s^{-1}$ and $\beta^0 = 65.0$ remains lower than 2.0. In fact, the flow rates of the supersaturated suspension stemmed from the T are low enough to allow a quasi-immediate consumption of the supersaturation by the crystals already present in the vessel.

Consequently, the nucleation is negligible in the stirred vessel and the number of crystals produced in the T-mixer is close to the final total number of crystals is given in Table 2. Fig. 5(A) gives the evolution of the simulated number of crystals along the mixing tube. We have also reported in this figure the experimental numbers of crystals obtained at the T-exit and deduced from the values of N_t given in Table 2 by taking into account the dilution. The great influence of the initial supersaturation ratio is well depicted by simulations: the experimental and predicted numbers of crystals increase with the same order of magnitude when the initial supersaturation ratio goes from 46.3 to 65.0.

As concerns the reactants flow rate, it can be seen in Fig. 5(A) that the simulated number of crystals increases continuously all along the T for $\beta^0 = 46.3$, even for the lowest flow rate. In that case, N_t is closely linked to the residence time. On the other hand, for $\beta^0 = 65.0$ and $Q_r = 2.36\,mm^3\,s^{-1}$, N_t reaches a plateau for times over 0.15 s. Nevertheless, these different trends are not observed experimentally. Finally, simulations indicates that secondary nucleation is negligible all along the experiment under such operating conditions.

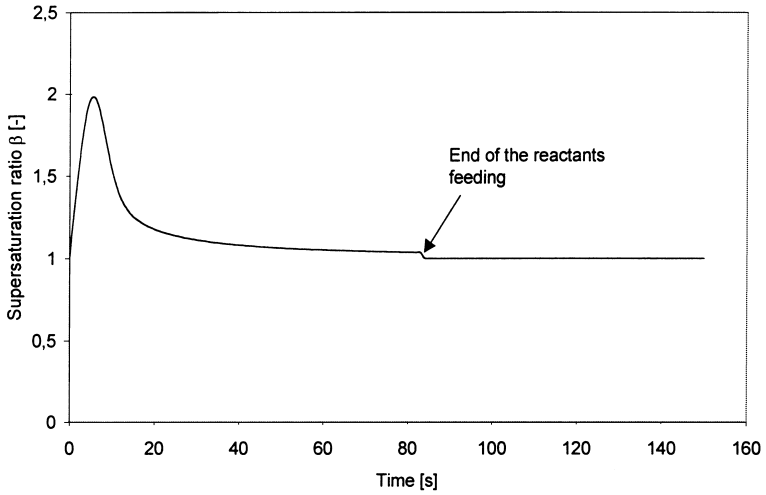

Fig. 6. Simulated supersaturation vs. time in the final stirred vessel: $\beta^0 = 65.0$, $Q_r = 4.80\,mm^3\,s^{-1}$.

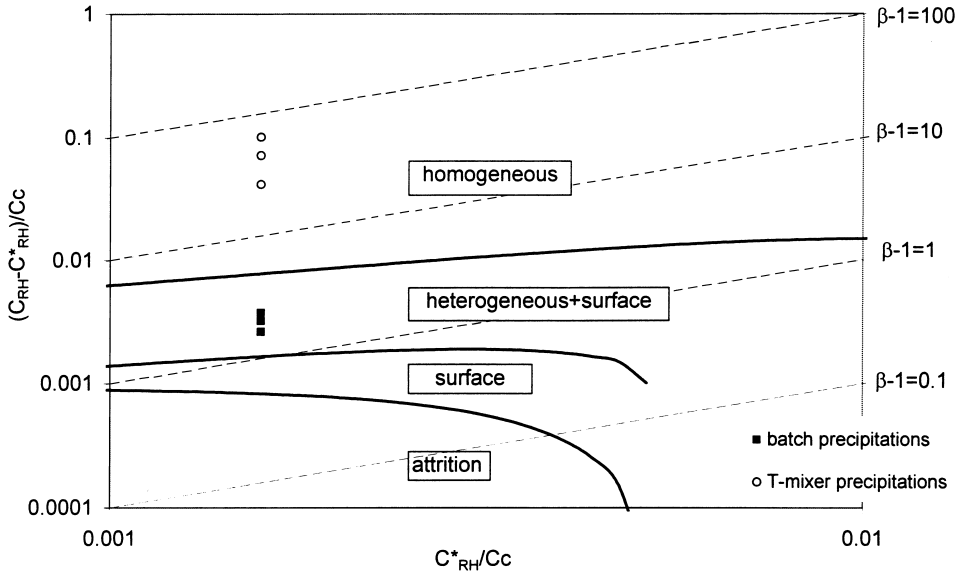

Fig. 7. Dimensionless metastable supersaturation against the dimensionless solubility with areas in which *attrition* controlled nucleation, *surface* controlled nucleation, surface controlled nucleation with a contribution of *heterogeneous* primary nucleation and *homogeneous* primary nucleation are dominant [6].

3.3. Ranges of supersaturation with dominant nucleation mechanisms

The kinetic laws (sets $\mathcal{A}$ and $\mathcal{B}$) allow one to estimate the metastable zones widths of the different nucleation mechanisms [6]. The diagram presented in Fig. 7 is based on the kinetic laws obtained in this work at 25°C. The influence of the temperature is estimated by mean of the energies of activation proposed by Mersmann [6]. To each zone corresponds a dominant nucleation mechanism.

We have also reported in Fig. 7 the points relative to the batch and the T-mixer precipitations. It is clear that only the homogeneous primary nucleation can be identified in the T-mixer experiments, whereas the perfectly mixed batch reactor experiments are well adapted to determine the heterogeneous primary nucleation and secondary nucleation kinetic parameters. Besides, as seen before, the integration growth kinetics under high supersaturation can be identified from the T-mixer precipitations. Indeed, the small size of the crystals produced in the T-mixer, together with the high mixing lead to a growth mechanism controlled by integration. The integration growth kinetic under low supersaturation might be different from that obtained under high supersaturation as suggested by the BCF model [23]. Nevertheless, it cannot be determined from the batch experiments since crystal growth is then essentially diffusion controlled.

Finally, the complete set of kinetic parameters is found to be:

Nucleation :

$A_{\mathrm{Ihom}} = 12 \times 10^{17}(\mathrm{nb\,m^{-3}\,s^{-1}})$, $B_{\mathrm{Ihom}} = 80\,(-)$
$A_{\mathrm{Ihet}} = 0.55 \times 10^{9}(\mathrm{nb\,m^{-3}\,s^{-1}})$, $B_{\mathrm{Ihet}} = 4.4\,(-)$
$A_{\mathrm{II}} = 0.99 \times 10^{8}(\mathrm{nb\,m^{-2}\,s^{-1}})$, $B_{\mathrm{II}} = 4.8\,(-)$

Growth :

at high supersaturation $k_{\mathrm{c}} = 2.5\times10^{-4}\,\mathrm{m\,s^{-1}}$, j=1 (−),
in batch experiments : crystal growth essentially diffusion controlled.

4. Conclusion

According to these results, determining all the mechanisms and kinetics of precipitation of salicylic acid needs to prospect a large supersaturation domain. To do this, two experimental set-ups have been used. At low supersaturation, experiments were carried out in a stirred vessel whereas a T-mixer was used at high supersaturations to avoid mixing effects. The identification of precipitation kinetics in each case has clearly exhibited that the predominant mechanisms are functions of the supersaturation. Thus primary nucleation which was of heterogeneous type at low supersaturations turned into a homogeneous mechanism at high supersaturations. Secondary nucleation which played an important part at low supersaturations became negligible at high supersaturations. Likewise, crystal growth was essentially diffusion controlled at low supersaturations in the batch reactor and became sensitive to the surface integration kinetics at high supersaturations and under high mixing in the T-mixer. Obviously, it was then impossible to extrapolate T-mixer precipitations from batch experiments. Each kind of experiments has allowed to determine a limited number of kinetic parameters and only the global approach developed here has allowed to reach the complete kinetic model of salicylic acid precipitation.

References

[1] O. Söhnel, J. Garside, Precipitation, Basic Principles and Industrial Applications, Butterworths/Heinemann, Oxford, 1992.

[2] A. Mersmann, General prediction of statistically mean growth rates of a crystal collective, J. Crystal Growth 147 (1995) 181–193.

[3] N.S. Tavare, V.G. Gaikar, Precipitation of salicylic acid: hydrotropy and reaction, Ind. Eng. Chem. Res. 30 (1991) 722–728.

[4] R. Franck, R. David, J. Villermaux, J.P. Klein, Crystallization and precipitation engineering II. A Chemical reaction engineering approach to salicylic acid precipitation: modelling of batch kinetics and application to continuous operation, Chem. Eng. Sci. 43 (1988) 69–77.

[5] A. Al-Kayat, Reaction crystallization of salicylic acid, M.Sc. Thesis, Victoria University of Manchester, Manchester, 1988.

[6] A. Mersmann, Supersaturation and nucleation, Trans. IChemE 74 (1996) 812–820.

[7] T. Manth, D. Mignon, H. Offermann, Experimental investigation of precipitation reactions under homogeneous mixing conditions, Chem. Eng. Sci. 51 (1996) 2571–2576.

[8] M. Aoun, E. Plasari, R. David, J. Villermaux, A simultaneous determination of nucleation and growth rates from batch spontaneous precipitation, Chem. Eng. Sci. 54 (1999) 1161–1180.

[9] A. Eble, A. Mersmann, Interaction of kinetics governing the precipitation of nanoparticles, in: Proceedings of the 14th International Symposium on Industrial Crystallization, Cambridge, 1999.

[10] D. Mignon, T. Manth, H. Offermann, Kinetic modeling of batch precipitation reactions, Chem. Eng. Sci. 51 (1996) 2565–2570.

[11] V. Nallet, D. Mangin, J.P. Klein, Model identification of batch precipitations: application to salicylic acid, Comput. Chem. Eng. 22 (Suppl.) (1998) S649–S652.

[12] H.M. Hulburt, S. Katz, Some problems in particle technology. A statistical mechanical formulation, Chem. Eng. Sci. 19 (1964) 555.

[13] J.B. Rawlings, W.R. Witkowski, J.W. Eaton, Modelling and control of crystallizers, Powder Technol. 69 (1992) 3.

[14] B. Marcant, Méthodologie d'analyse d'un système de précipitation soumis à l'influence des conditions de mélange: cas de l'oxalate de calcium, Ph.D. Thesis, INPL, Nancy, France, 1992.

[15] P. Marchal, R. David, J.P. Klein, J. Villermaux, Crystallization and precipitation engineering — I. An efficient method for solving population balance in crystallization with agglomeration, Chem. Eng. Sci. 43 (1988) 59–67.

[16] V. Nallet, Fabrication de microparticules d'acide salicylique par précipitation en mélangeur en T: étude expérimentale, modélisation et séparation par agglomération en phase liquide, Ph.D. Thesis, UCB, Lyon 1, Lyon, France, 1997.

[17] R. Geisler, A. Mersmann, H. Voit, Macro- and micromixing in stirred tanks, Int. Chem. Eng. 31 (1991) 642–653.

[18] V. Nallet, D. Mangin, J.P. Klein, Modelling of the kinetics of salicylic acid precipitation in batch precipitator, in: Proceedings of the CGOM, BIWIC, Bremen, Germany, 1997.

[19] A.E. Nielsen, Kinetics of Precipitation, Pergamon Press, Oxford, 1964.

[20] J. Garside, Industrial crystallisation from solution, Chem. Eng. Sci. 40 (1995) 3–26.

[21] G. Herndl, A. Mersmann, Fluid dynamics and mass-transfer in stirred suspensions, Chem. Eng. Commun. 13 (1981) 23–37.

[22] P.M. Armenante, D.J. Kirwan, Mass transfer to microparticles in agitated vessel, Chem. Eng. Sci. 44 (12) (1989) 2781–2796.

[23] W.K. Burton, N. Cabrera, F.C. Franck, The growth of crystals and the equilibrium structure of their surfaces, Phil. Trans. R. Soc. London A4243 (1950/1951) 299–358.